nature structural & molecular biology

Nα-acetylated Sir3 stabilizes the conformation of a nucleosome-binding loop in the BAH domain

Dongxue Yang[1–3], Qianglin Fang[1–3], Mingzhu Wang[1,3], Ren Ren[1], Hong Wang[1,2], Meng He[1], Youwei Sun[1], Na Yang[1] & Rui-Ming Xu[1]

In *Saccharomyces cerevisiae*, acetylation of the Sir3 N terminus is important for transcriptional silencing. This covalent modification promotes the binding of the Sir3 BAH domain to the nucleosome, but a mechanistic understanding of this phenomenon is lacking. By X-ray crystallography, we show here that the acetylated N terminus of Sir3 does not interact with the nucleosome directly. Instead, it stabilizes a nucleosome-binding loop in the BAH domain.

Silencing of the mating-type (*HM*) and telomeric loci requires the set of *trans*-acting silent information regulators Sir1, Sir2, Sir3 and Sir4. The Sir proteins are recruited to the *HM* and telomeric loci through interaction with silencer-bound proteins[1]. Sir1 interacts with the BAH domain of Orc1, the largest subunit of the hexameric ORC complex, and also with Sir4 (refs. 2–6). Sir2, Sir3 and Sir4 form a multimeric complex that spreads across the chromatin domain flanked by silencers, thus resulting in the formation of a repressive chromatin structure[1,7–9].

Sir3 also has an N-terminal BAH domain, which is essential for Sir3's silencing function[10,11]. Overexpression of the BAH domain without the rest of the Sir3 protein can achieve silencing if Sir1 is also overexpressed[11]. Notably, the silencing function of Sir3 or its BAH domain depends on the acetylation of the terminal α-amino group[12]. In budding yeast, the initiating methionine of Sir3 is removed, and the following residue, Ala2, is Nα-terminally acetylated by the Ard1–Nat1 acetyltransferase complex. Changing Ala2 to a residue that interferes with the removal of the methionine or one that renders the N terminus unsuitable for acetylation results in defective silencing[12]. The acetylation-dependent silencing property of Sir3 and its BAH domain is reflected in their nucleosome binding behavior. Nα acetylation of Ala2 greatly increases Sir3's nucleosome binding affinity[13,14]. The structure of the Sir3 BAH domain in complex with the nucleosome core particle (NCP) has recently been determined[15]; however, the bacterially expressed Sir3 BAH domain used for cocrystallization was unacetylated, thus leaving unanswered the question of how Nα acetylation of the Sir3 BAH domain affects NCP binding.

We set out to investigate the role of Nα acetylation of the Sir3 BAH domain in NCP binding. We used baculovirus-infected insect cells to produce Nα-acetylated Sir3 BAH domain ($Sir3^{BAH}$, amino acids (aa) 1–219) and a D205N hypermorphic mutant ($Sir3^{BAH\_D205N}$). We confirmed the acetylation of Ala2 of the recombinant proteins by MS analysis (**Supplementary Fig. 1**) and cocrystallized $Sir3^{BAH\_D205N}$ with NCP reconstituted with bacterially expressed yeast histones and 146-base-pair α-satellite DNA (hereafter termed the $acSir3^{BAH\_D205N}$–yNCP complex). As previously reported[13,14], both the N-terminal acetylation and the D205N mutation increased the binding of the Sir3 BAH domain to the nucleosome, as judged by isothermal titration calorimetry (ITC) measurements with purified $Sir3^{BAH}$ proteins and *in vitro*–reconstituted yeast mononucleosomes (**Supplementary Fig. 2**). The K_d values for unacetylated and acetylated wild-type BAH domains are 10.7 μM and 0.36 μM, respectively, and the corresponding values for the D205N mutant are 0.24 μM and 0.04 μM, respectively. Hence, Ala2 acetylation increased the NCP binding affinity by ~30 fold, a level comparable to the ~45-fold increase introduced by the D205N mutation.

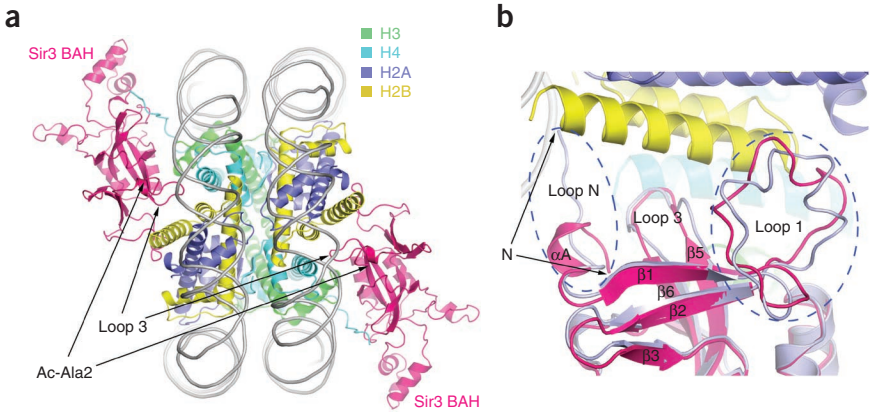

Figure 1 Structure of the Sir3 BAH domain in complex with NCP. (**a**) Ribbon diagram showing the overall structure of the $acSir3^{BAH\_D205N}$–yNCP complex. (**b**) Structural differences between the NCP-bound acetylated and unacetylated Sir3 BAH domains. The two main regions of difference, loop N and loop 1, are highlighted with dashed-line ovals. The superimposed unacetylated Sir3 BAH domain is shown in light blue.

[1]National Laboratory of Biomacromolecules, Institute of Biophysics, Chinese Academy of Sciences, Beijing, China. [2]University of Chinese Academy of Sciences, Beijing, China. [3]These authors contributed equally to this work. Correspondence should be addressed to N.Y. (yangna@moon.ibp.ac.cn) or R.-M.X. (rmxu@sun5.ibp.ac.cn).

Received 21 January; accepted 21 June; published online 11 August 2013; doi:10.1038/nsmb.2637

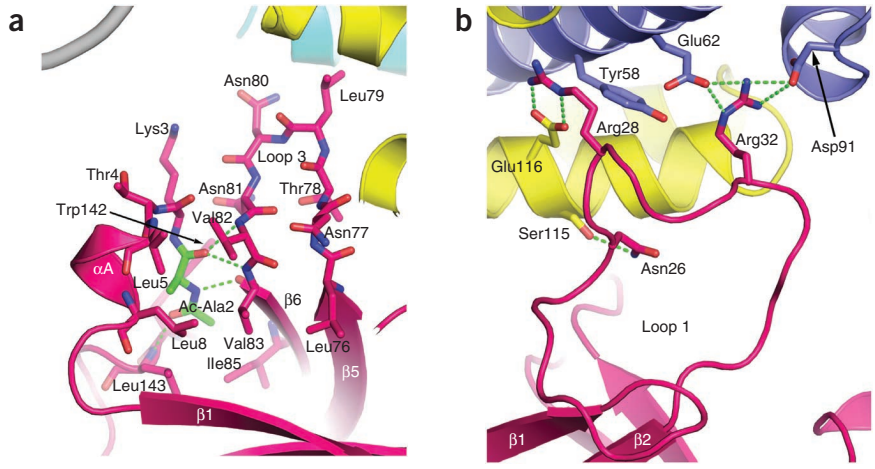

Figure 2 Intra- and intermolecular interactions of the acetylated N terminus and loop 1 of the Sir3 BAH domain. (**a**) Hydrogen bonds (green dashed lines) between ac-Ala2 and the surrounding Sir3 residues. (**b**) Detailed view of intermolecular hydrogen bonds between loop-1 residues of the Sir3 BAH domain and residues in histones H2A (blue) and H2B (yellow).

The structure showed that two molecules of the Sir3 BAH domain bound pseudosymmetrically to one NCP (**Fig. 1a**). The BAH domain contacted all four histones from the NCP, and the overall binding mode was similar to that observed in the structure of the bacterially expressed D205N mutant of Sir3^{BAH} in complex with the NCP reconstituted with *Xenopus* histones and 601 DNA, hereafter referred to as the Sir3^{BAH_D205N}–xNCP complex[15]. There were two main differences between the two structures (**Fig. 1b**). First, the N-terminal end of the acetylated BAH domain, acetylated Ala2 (ac-Ala2), turned back toward αA and inserted into a pocket between αA and β6 in Sir3^{BAH} (**Fig. 1b** and **Supplementary Fig. 3a**,**b**). In the unacetylated Sir3^{BAH_D205N}–xNCP complex, the N-terminal loop (loop N) adopted an extended conformation, with the N-terminal end positioned near the NCP (**Fig. 1b**). Second, the loop connecting β1 and β2 (loop 1) was well ordered in the acSir3^{BAH_D205N}–yNCP structure (**Fig. 1b** and **Supplementary Fig. 3c**), whereas this loop in the Sir3^{BAH_D205N}–xNCP complex could not be reliably positioned.

Ac-Ala2 was tightly locked in a hydrophobic pocket formed by residues from αA, β6, loop 3 and the loop connecting β7 and β8 in Sir3^{BAH} (**Fig. 2a**). The carbonyl oxygen of the acetyl group of ac-Ala2 made a hydrogen bond with the amide group of Leu143 located on the β7–β8 loop, whereas the amide and the carbonyl groups of ac-Ala2 made three antiparallel β-sheet–like hydrogen bonds with the carbonyl and amide groups of Val83 and Val82 on β6 and loop 3, respectively (**Fig. 2a**). The hydrophobic acetyl group of ac-Ala2 was immediately surrounded by hydrophobic residues Leu8 from αA, Trp142 and Leu143 from the β7–β8 loop and Val83 and Ile85 from β6 (**Fig. 2a**). An unacetylated Ala2 is unlikely to bind in this manner, as it would be energetically unfavorable to place the positively charged amino group in the hydrophobic pocket. The ordered loop 1 of Sir3^{BAH} interacted directly with NCP. Asn26 and Arg28 of Sir3^{BAH} made hydrogen bonds with Ser115 and Glu116 of histone H2B, respectively (**Fig. 2b**). Arg28 of Sir3^{BAH} also made van der Waals and hydrophobic interactions with histone H2A, notably through Tyr58. In addition, Arg32 of Sir3^{BAH} interacted with two negatively charged residues of histone H2A, Glu62 and Asp91.

To determine whether the positioning of ac-Ala2 was due to acetylation or NCP binding, we also crystallized acetylated Sir3^{BAH} without NCP. The 1.85-Å apo-acSir3^{BAH} structure showed that ac-Ala2 was located in exactly the same position as in the complex structure with NCP (**Fig. 3a** and **Supplementary Fig. 4a**,**b**). However, loop 1 was disordered in the protein-alone structure. This observation indicated that it was the acetylation of Ala2, but not NCP binding, that caused ac-Ala2 to fold back. In contrast, the conformation of loop 1 in the acSir3^{BAH_D205N}–yNCP complex was induced by NCP binding.

Ac-Ala2 did not directly interact with NCP. Comparison of the structure of acSir3^{BAH} with two previously reported structures of unacetylated Sir3 BAH domain revealed how N-terminal acetylation helped NCP binding. Loop 3, which was closely juxtaposed with the acetylated N terminus of the Sir3 BAH domain and critical for interaction with histones H4 and H2B from the NCP (**Fig. 1a**,**b**), is disordered in the unacetylated Sir3 BAH domain structures (**Supplementary Fig. 5a**)[11,15,16]. In contrast, loop 3 was well ordered in the apo structure of acSir3^{BAH}, and its conformation closely resembled that in the NCP-bound structure (**Fig. 3a**). A plausible model is that acetylation of Ala2 stabilizes loop 3 in a conformation for productive interaction with the nucleosome. A previous genetic screen revealed that an N80D substitution in loop 3 caused silencing defects at the telomeric and *HML* loci and implicated the role of loop 3 in NCP interaction[14]. To biochemically test the importance of loop-3 residues in NCP binding, we changed Leu79 and Asn80 of Sir3^{BAH} to a pair of alanines and expressed the L79A N80A (AA) mutant in insect cells. Our electrophoretic mobility shift assay indicated that the NCP binding ability of the mutant protein was markedly reduced, thus confirming that loop 3 is crucial for NCP binding (**Fig. 3b**). Furthermore, we reasoned that changing Val83 to a proline (V83P) should disrupt the hydrogen bonds and reduce the hydrophobic interaction between ac-Ala2 and its binding environment in Sir3^{BAH} (**Fig. 2a**). As a consequence, it is predicted that the V83P mutation will destabilize loop 3 and affect the NCP binding ability. Indeed, the V83P mutant lost its ability to bind NCP (**Fig. 3b**), and, as predicted,

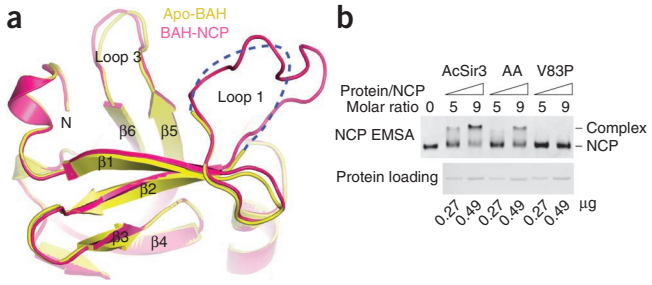

Figure 3 Acetylation of Ala2 stabilizes the conformation of the NCP-binding loop 3. (**a**) Superposition of the NCP-bound (pink) and apo (yellow) structures of the acetylated Sir3 BAH domain. A blue dashed-line segment indicates the disordered loop-1 region in the apo structure. (**b**) Polyacrylamide-gel electrophoretic mobility shift assay analyses of NCP binding (top). Insect cell–expressed wild-type (acSir3), L79A N80A (AA) and V83P mutants of Sir3^{BAH} were added in five- or nine-fold molar excess, as shown in the Coomassie blue–stained SDS-PAGE gel indicating loading (bottom). Original images of gels can be found in **Supplementary Figure 6**.

both the N-terminal loop and loop 3 became disordered in the structure of the V83P mutant (**Supplementary Fig. 5b**). These results support the model that Ala2 acetylation strengthens the interaction between $Sir3^{BAH}$ and NCP by stabilizing loop 3 of $Sir3^{BAH}$ in a productive conformation.

This role of promoting nucleosome interaction by N-terminal acetylation is likely to operate in the BAH domain of Orc1 as well, because the two BAH domains share extensive sequence homology, and their first eight amino acids are identical. Furthermore, the Orc1 BAH domain's ability to bind the nucleosome also depends on the acetylation of Ala2 (refs. 12,13,17). Most eukaryotic proteins are acetylated at the N terminus, but the biological function of this common modification in eukaryotes is diverse and not well understood[18]. A couple of recent studies reported the direct involvement of an N-terminal acetyl group in intermolecular interactions[19,20]. Together with the varied theme found here, they offer insights into the structure and function of the vast eukaryotic N-terminal acetylome.

METHODS

Methods and any associated references are available in the online version of the paper.

Accession codes. Atomic coordinates and structural factors for the $acSir3^{BAH\_D205N}$–yNCP, apo-$acSir3^{BAH}$ and $acSir3^{BAH\_V83P}$ structures have been deposited in the Protein Data Bank, under accession codes 4KUD, 4KUI and 4KUL, respectively.

Note: Any Supplementary Information and Source Data files are available in the online version of the paper.

ACKNOWLEDGMENTS

We thank Shanghai Synchrotron Radiation Facility beamline scientists for technical support during data collection and F. Yang and staff scientists at the protein science core facility at the Institute of Biophysics for help with MS analyses. This work was supported by grants from the Chinese Ministry of Science and Technology (2009CB825501 to R.-M.X.) and the Natural Science Foundation of China (90919029, 3098801 and 31210103914 to R.-M.X.).

AUTHOR CONTRIBUTIONS

D.Y. and Q.F. designed and performed experiments, analyzed data and wrote the paper. M.W. carried out structure determination, analyzed data and wrote the paper. R.R., H.W., M.H. and Y.S. participated in the experiments. N.Y. and R.-M.X. designed experiments, analyzed data and wrote the paper.

COMPETING FINANCIAL INTERESTS

The authors declare no competing financial interests.

1. Rusche, L.N., Kirchmaier, A.L. & Rine, J. *Annu. Rev. Biochem.* **72**, 481–516 (2003).
2. Bell, S.P., Mitchell, J., Leber, J., Kobayashi, R. & Stillman, B. *Cell* **83**, 563–568 (1995).
3. Triolo, T. & Sternglanz, R. *Nature* **381**, 251–253 (1996).
4. Hsu, H.C., Stillman, B. & Xu, R.M. *Proc. Natl. Acad. Sci. USA* **102**, 8519–8524 (2005).
5. Hou, Z., Bernstein, D.A., Fox, C.A. & Keck, J.L. *Proc. Natl. Acad. Sci. USA* **102**, 8489–8494 (2005).
6. Yang, N. & Xu, R.M. *Crit. Rev. Biochem. Mol. Biol.* **48**, 211–221 (2013).
7. Hecht, A., Strahl-Bolsinger, S. & Grunstein, M. *Nature* **383**, 92–96 (1996).
8. Hoppe, G.J. *et al. Mol. Cell Biol.* **22**, 4167–4180 (2002).
9. Rusché, L.N., Kirchmaier, A.L. & Rine, J. *Mol. Biol. Cell* **13**, 2207–2222 (2002).
10. Gotta, M., Palladino, F. & Gasser, S.M. *Mol. Cell Biol.* **18**, 6110–6120 (1998).
11. Connelly, J.J. *et al. Mol. Cell Biol.* **26**, 3256–3265 (2006).
12. Wang, X., Connelly, J.J., Wang, C.L. & Sternglanz, R. *Genetics* **168**, 547–551 (2004).
13. Onishi, M., Liou, G.G., Buchberger, J.R., Walz, T. & Moazed, D. *Mol. Cell* **28**, 1015–1028 (2007).
14. Sampath, V. *et al. Mol. Cell Biol.* **29**, 2532–2545 (2009).
15. Armache, K.J., Garlick, J.D., Canzio, D., Narlikar, G.J. & Kingston, R.E. *Science* **334**, 977–982 (2011).
16. Hou, Z., Danzer, J.R., Fox, C.A. & Keck, J.L. *Protein Sci.* **15**, 1182–1186 (2006).
17. Zhang, Z., Hayashi, M.K., Merkel, O., Stillman, B. & Xu, R.M. *EMBO J.* **21**, 4600–4611 (2002).
18. Arnesen, T. *et al. Proc. Natl. Acad. Sci. USA* **106**, 8157–8162 (2009).
19. Monda, J.K. *et al. Structure* **21**, 42–53 (2013).
20. Scott, D.C., Monda, J.K., Bennett, E.J., Harper, J.W. & Schulman, B.A. *Science* **334**, 674–678 (2011).

ONLINE METHODS

Preparation of the BAH domain of Sir3, NCP and their complex. The BAH domain of Sir3 (aa 1–219) and its D205N, L79A N80A, and V83P mutants were expressed as a C-terminal hexahistidine fusion protein in Sf9 cells with the Bac-to-Bac Baculovirus Expression System (Invitrogen) according to the procedures recommended by the manufacturer. The corresponding N-terminal-nonacetylated proteins were expressed as a C-terminal poly(His)-tagged protein in the BL21(DE3)-RIL strain of *E. coli* with the pET-22b vector (Novagen). Recombinant proteins were purified with Ni-chelating and size-exclusion column chromatography. NCP made of bacterially expressed *S. cerevisiae* histones H2A, H2B, H3 and H4 and a 146-bp palindromic DNA fragment derived from human α-satellite DNA was prepared according to a described procedure[21]. The acSir3^{BAH_D205N}–yNCP complex was prepared by mixture of the BAH domain with NCP, in a 3:1 molar ratio, and subsequent separation of the free BAH domain with a Superdex 200 10/300 GL gel-filtration column (GE Healthcare) in a buffer containing 20 mM Tris, pH 7.4, 50 mM KCl and 1 mM DTT.

Mass spectrometry analysis. Sir3^{BAH} (25 μg) purified from Sf9 cells was denatured in 20 μl buffer containing 8 M urea, 50 mM NH_4HCO_3 and 10 mM DTT for an hour. Next, 40 mM iodoacetamide was added and the mixture incubated at room temperature in the dark for an hour to block the sulfhydryl group. Afterward, excessive iodoacetamide was neutralized by addition of DTT. The protein sample was then diluted with 50 mM NH_4HCO_3 to lower the urea concentration to <2 M for overnight proteolytic digestion with 0.5 μg of Arg-C at 37 °C. The proteolytic reaction was stopped by the addition of formic acid to a final concentration of 0.1%.

The Arg-C–generated peptides were analyzed by LC-MS/MS with a Thermo Fisher Finnigan LTQ linear ion trap mass spectrometer in line with a Finnigan Surveyor MS Pump Plus HPLC system. A gradient of 0–80% acetonitrile at a flow rate of 500 nL min^{-1} was used to elute the peptides from the trap column (300SB-C18, 5 × 0.3 mm, 5 μm particle; Agilent) connected to a self-packed analytical column (C18, 100 μm i.d. × 100 mm, 3 μm particle; SunChrom). The eluted peptides were introduced online into the mass spectrometer with nanoelectrospray ionization (ESI). The five most abundant ions (one microscan per spectrum; precursor isolation width 1.0 *m/z*, 35% collision energy, 30 ms ion activation, 90 s exclusion duration and 1 repeat count) were selected from a full-scan mass spectrum for fragmentation by collision-induced dissociation (CID). The mass data were analyzed with SEQUEST for the identification of peptide fragments.

Crystallization, data collection, structure determination and refinement. The acSir3^{BAH_D205N}–yNCP complex at a concentration of ~4–6 mg ml^{-1} was crystallized in a buffer condition containing 0.1 M KCl, 0.01 M $CaCl_2$, 16% PEG 400 and 0.05 M sodium citrate (pH 4.8). The wild-type acSir3^{BAH}, at a concentration of ~10 mg ml^{-1}, was crystallized in a condition with 0.2 M $CaCl_2$, 0.1 M sodium acetate, pH 4.6, and 18% 2-propanol; acSir3^{BAH_V83P} was crystallized in a similar condition, with 14% 2-propanol instead. All of the crystals were grown at 16 °C.

X-ray diffraction data were collected with a Quantum 315r CCD detector (ADSC) at Beamline BL17U of the Shanghai Synchrotron Radiation Facility. Cryogenic data collection at 100 K for the acSir3^{BAH_D205N}–yNCP complex crystal used a cryoprotectant with 10% glycerol added to its crystallization well solution, and that for the apo acSir3^{BAH} and acSir3^{BAH_V83P} crystals used a cryoprotectant with 20% glycerol. The data for the acSir3^{BAH_D205N}–yNCP complex, acSir3^{BAH} and acSir3^{BAH_V83P} crystals were collected at a wavelength of 0.9788 Å, 0.9760 Å and 0.9789 Å, respectively, and processed with HKL2000 (ref. 22). The NCP complex structure was solved by molecular replacement with Molrep[23], with the yeast NCP structure (PDB 1ID3 (ref. 24)) and the Sir3 BAH domain structure (PDB 2FVU (ref. 11)) as the search models. The acSir3^{BAH} structure was solved by molecular replacement with Phaser[23], with the structure of the Sir3 BAH domain (PDB 2FVU) as the search model. The structures were refined with PHENIX[25] and COOT[26]. The refined model of the acSir3^{BAH_D205N}–yNCP complex has R_{work} and R_{free} values of 19.8% and 23.7%, respectively, and 97.1% of the residues are in the favored regions of the Ramachandran plot, with none in the disallowed regions. Detailed statistics for the crystallographic analyses are shown in **Supplementary Table 1**.

Isothermal titration calorimetry measurements. All ITC experiments were performed at 25 °C with an ITC200 calorimeter (MicroCal LLC). For each experiment, 20 injections of 2 μl each were made. Various Sir3^{BAH} proteins were individually titrated into a 200-μl cell filled with yNCP in the same buffer. Each injection took place in 4 s, with a 2-min interval between subsequent injections, while the sample cell was stirred at 600 r.p.m. For the bacterially expressed Sir3^{BAH} and Sir3^{BAH_D205N}, protein solutions at concentrations of 0.8 mM and 0.18 mM were titrated into yNCP solutions at 0.03 mM and 0.018 mM concentrations in the buffer with 20 mM Tris-HCl, pH 7.4, and 100 mM KCl, respectively. For the insect cell–expressed acetylated Sir3^{BAH} and Sir3^{BAH_D205N}, protein concentrations of 0.4 mM and 0.2 mM were used to titrate into a 0.024 mM yNCP solution in the buffer with 20 mM HEPES, pH 7.4, and 100 mM KCl. Background heat measured without added protein was subtracted from the integrated data, and the data were analyzed by nonlinear least-squares fitting with a single-binding-site (two independent, identical binding sites) model with ORIGIN 7.0 (OriginLab).

Gel-shift assay. yNCP (0.44 μg; 2.2 pM) was mixed with acetylated and non-acetylated Sir3^{BAH} and Sir3^{BAH_D205N} samples at varying protein/NCP molar ratios in a buffer containing 20 mM Tris-HCl, pH 7.5, 100 mM NaCl, 0.5 mM EDTA and 5% glycerol. The mixtures were incubated at room temperature for 0.5 h before analysis by native gel electrophoresis run at 150 V and at 4 °C with 0.25× TBE, with an 8% polyacrylamide gel. Gels were stained with GoldView. Original images used in this study can be found in **Supplementary Figure 6**.

21. Luger, K., Rechsteiner, T.J., Flaus, A.J., Waye, M.M. & Richmond, T.J. *J. Mol. Biol.* **272**, 301–311 (1997).
22. Otwinowski, Z. & Minor, W. *Methods Enzymol.* **276**, 307–326 (1997).
23. Collaborative Computational Project. *Acta Crystallogr. D Biol. Crystallogr.* **50**, 760–763 (1994).
24. White, C.L., Suto, R.K. & Luger, K. *EMBO J.* **20**, 5207–5218 (2001).
25. Adams, P.D. *et al. Acta Crystallogr. D Biol. Crystallogr.* **66**, 213–221 (2010).
26. Emsley, P. & Cowtan, K. *Acta Crystallogr. D Biol. Crystallogr.* **60**, 2126–2132 (2004).